Research Article | Vol. 29, No. 26 / 20 Dec 2021 / Optics Express 42827

Optics EXPRESS

Topological states in the super-SSH model

YIQI ZHANG,[1] BOQUAN REN,[1] YONGDONG LI,[1] AND FANGWEI YE[2,*]

[1] *Key Laboratory for Physical Electronics and Devices of the Ministry of Education & Shaanxi Key Lab of Information Photonic Technique, School of Electronic Science and Engineering, Xi'an Jiaotong University, Xi'an 710049, China*

[2] *School of Physics and Astronomy, Shanghai Jiao Tong University, Shanghai 200240, China*

[*] *fangweiye@sjtu.edu.cn*

Abstract: The topological edge state distributes along the edge of a topological insulator which has advantages in prohibiting radiation and reflection in the evolution dynamics because of the topological protection property. The Su-Schrieffer-Heeger (SSH) model provides the simplest lattice configuration that supports topological edge states. Here, we investigate the properties of an extended SSH model – *super-SSH model* – with three sites in a unit cell for one-dimensional case and nine sites in a unit cell for two-dimensional case. Theoretical analysis and numerical simulation demonstrate that topological edge states and topological defect states are supported in the super-SSH model. This work extends the form of SSH model and may serve as a novel platform for developing photonic techniques based on topological phase transition.

1. Introduction

The topological insulator is a new kind of matter that supports current conduction only on the surface with the bulk being completely insulated [1,2]. Due to its fascinating properties and potential applications, investigations on topological insulators have been attracting increasing interest and exhibiting a prosperous development. Among the various theoretical research models of topological insulators, perhaps the simplest model is the well established one-dimensional Su-Schrieffer-Heeger (SSH) model [3]. The SSH model considers a periodic array with two sites in one unit cell, and the coupling between intracell sites alternates with the coupling between intercell sites. As a result, the SSH structure exhibits two topologically different phases, one being topological trivial and the other being nontrivial. At the interface between two topologically different chains or at the truncated edge of the topologically nontrivial chain, localized interfacial or edge mode exists. Thus far, the SSH model has been implemented in various physical branches such as in photonics [4–15], in acoustics [16,17], in ultracold matters [18–20], and in quantum information [21,22]. In addition, the SSH model is also discussed in the non-Hermitian [23–28] and nonlinear [29–33] regimes, as well as in the fabricating and elucidating higher-order topological insulators [34–37].

Above-mentioned works were all concerned with structures with two sites in a unit cell, and here we propose a variant of SSH model in which there are *three* sites in a unit cell. To distinguish this novel SSH model from the standard SSH model, we name it as a *super-SSH model*. The purpose of the establishment of such a super-SSH model is two folded. First, there are a variety of advanced lattices such as Lieb lattice, Kagome lattice and lattice with type-II Dirac cone [38–40] that possess three sites in one unit cell. These lattices are useful and play important roles in promoting development of photonic techniques. Another reason is that the one-dimensional super-SSH model itself may exhibits interesting properties that are distinct from those of the standard SSH model and yet to be explored. Recently, we find similar work about extended SSH model [41,42], in which the super-SSH model is involved. However, the distinction here is also evidently: Firstly, we only consider the case with equal intracell and intercell couplings

#445301 https://doi.org/10.1364/OE.445301
Journal © 2021 Received 7 Oct 2021; revised 20 Nov 2021; accepted 27 Nov 2021; published 8 Dec 2021

Optics EXPRESS

that are much simpler. Secondly, we carry out our investigation based on both discrete model and continuous model that is much closer to the real world. Last but not least, we extend our discussion to two-dimensions which may provide a novel platform for generating corner laser [36,43–45].

2. Analytical analysis based on the tight-binding method

2.1. One-dimensional case

The super-SSH model considered here is schematically shown in Fig. 1(a): a period array composed of coupled trimers, the coupling between neighboured trimers being w while the coupling between sites inside trimers being v_1 and v_2 respectively. However, for the simplicity we let $v_1 = v_2 = v$. Obviously, when such trimer structure is truncated, the resultant structure may have three different cases [Figs. 1(b)–1(d)]. In the following we start from the tightly-binding method to analyze analytically the super-SSH model, and then go to its optical realization.

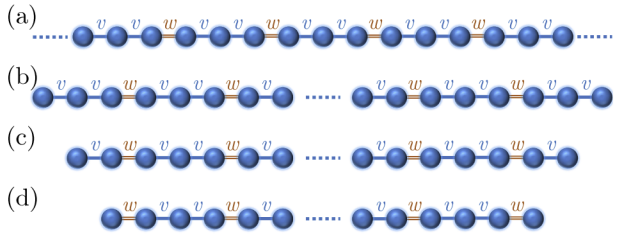

Fig. 1. Scheme of super-SSH model. Hopping strength is staggered: intracell hopping v (blue thick lines) is different from intercell hopping w (orange double lines). (a) A super-SSH chain with periodic boundary condition. (b)-(d) Super-SSH chains with open boundary conditions.

With reference to the schematic structure shown in Fig. 1(a), the momentum-space Hamiltonian of the periodic super-SSH chain can be written as the following 3×3 matrix,

$$\mathcal{H} = \begin{bmatrix} 0 & v & we^{-ik} \\ v & 0 & v \\ we^{ik} & v & 0 \end{bmatrix}. \tag{1}$$

The corresponding eigenvalues of Eq. (1) is given explicitly as,

$$\varepsilon_1 = \frac{p}{\sqrt[3]{q + \sqrt{q^2 - p^3}}} + \sqrt[3]{q + \sqrt{q^2 - p^3}}, \tag{2}$$

$$\varepsilon_2 = -\frac{pe^{i\pi/3}}{\sqrt[3]{q + \sqrt{q^2 - p^3}}} - e^{-i\pi/3}\sqrt[3]{q + \sqrt{q^2 - p^3}}, \tag{3}$$

$$\varepsilon_3 = -\frac{pe^{-i\pi/3}}{\sqrt[3]{q + \sqrt{q^2 - p^3}}} - e^{i\pi/3}\sqrt[3]{q + \sqrt{q^2 - p^3}}, \tag{4}$$

with $p = (2v^2 + w^2)/3$ and $q = v^2 w \cos(k)$. Here, k is the wavenumber that takes values from the first Brillouin zone (BZ). In Fig. 2(a), we display eigenvalues $\varepsilon_i\,(i = 1, 2, 3)$ versus k, for some

Optics EXPRESS

typical values of v and w. Note that, if the intercell hopping is equal to the intracell hopping (viz. $v = w$), the whole array is simplified into a homogeneous periodic structure, for which the first and the second bands interact at $k = \pm\pi$, and the second the third band interact at $k = 0$. As soon as the intercell couplings differs from the intracell ones (viz. $v \neq w$), the gap between the band 1 and 2, and that between the band 2 and 3, opens. This situation is quite similar to the standard SSH model [3], although the trimer array considered here involves three bands and two gaps. Note, however, in contrast to the standard SSH model that respects the chiral symmetry, that is, the band structure is exactly the same when reflected about the mid-point of the gap or swap the role of w and v, the trimer model obviously lacks the chiral symmetry, and the band structure changes when w and v is exchanged. The latter point is readily clear by considering two opposite cases at the extreme, ($v = 0,\ w = 1$) versus ($v = 1,\ w = 0$). The former yields top and bottom bands at $\varepsilon = \pm 1$ while the latter at $\varepsilon = \pm\sqrt{2}$.

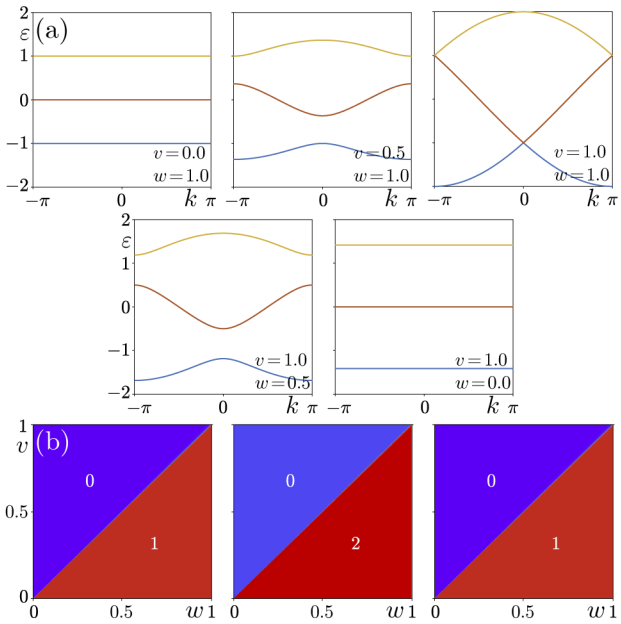

Fig. 2. (a) Dispersion relation of the one-dimensional super-SSH model, Eqs. (2)-(4), for five settings of hopping amplitude that are given at the right-bottom corner of each panel. From top to bottom, the eigenvalues are ε_1, ε_2 and ε_3, respectively. (b) Winding number of the three bands by scanning v and w.

We characterize the topological property of the super-SSH model by calculating the winding number of each band, which is defined as [46]

$$\gamma = \frac{i}{2\pi}\int_{\mathrm{BZ}} \langle u(k)|\partial_k|u(k)\rangle dk, \tag{5}$$

where $|u(k)\rangle$ represents the eigenstate of a particular band of the bulk momentum-space Hamiltonian (1). By changing the values of v and w between 0 and 1, we obtain the winding number of the first three bands, as shown in Fig. 2(b). Same to the case of the standard SSH model the winding number of the first and the third band of the super-SSH model is also either 0 or 1: it is 1 if $w>v$ and 0 if $w<v$. In addition, here we have a middle band, whose winding number is either 2 ($w>v$) or 0 ($w<v$).

Optics EXPRESS

2.2. Two-dimensional case

We generalize the 1D super-SSH model into 2D, for which one sees a 1D super-SSH model in both horizontal and vertical directions (Fig. 3). This 2D super-SSH structure has nine sites in each unit cell, thus, its bulk Hamiltonian can be written as

$$\mathcal{H} = \begin{bmatrix} 0 & v & we^{-ik_x} & v & 0 & 0 & we^{ik_y} & 0 & 0 \\ v & 0 & v & 0 & v & 0 & 0 & we^{ik_y} & 0 \\ we^{ik_x} & v & 0 & 0 & 0 & v & 0 & 0 & we^{ik_y} \\ v & 0 & 0 & 0 & v & we^{-ik_x} & v & 0 & 0 \\ 0 & v & 0 & v & 0 & v & 0 & v & 0 \\ 0 & 0 & v & we^{ik_x} & v & 0 & 0 & 0 & v \\ we^{-ik_y} & 0 & 0 & v & 0 & 0 & 0 & v & we^{-ik_x} \\ 0 & we^{-ik_y} & 0 & 0 & v & 0 & v & 0 & v \\ 0 & 0 & we^{-ik_y} & 0 & 0 & v & we^{ik_x} & v & 0 \end{bmatrix}, \tag{6}$$

where $k_{x,y}$ is the wavenumber taking values in the first BZ of the lattice, $-\pi \leq k_{x,y} \leq \pi$. As done in the one-dimensional case, here we also show the band structure at five sets of v and w (Fig. 4). As expected, due to the dimension of the Hamiltonian (6), the system has nine bands (labelled as $\varepsilon_1 \sim \varepsilon_9$ from top to bottom). For either v or w being zero, all the nine bands are flat, and in addition, bands ε_2 and ε_3, bands ε_4, ε_5 and ε_6, as well as bands ε_7 and ε_8 are degenerated, respectively. If $v \neq w > 0$, the bands are not flat, and there are nodal lines due to the band crossing. While if $v = w = 1$ as shown in Fig. 4, all the bands coalesce with each other and band gaps disappear.

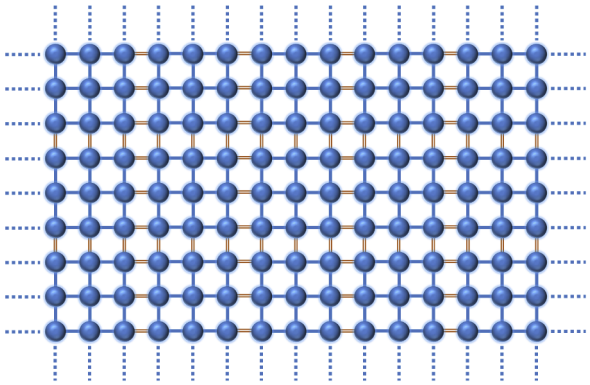

Fig. 3. Two-dimensional super-SSH model under periodic boundary condition.

For the two-dimensional case, the topological property of the system could be described by the polarized indices (p_x, p_y) [34], which are defined as

$$\begin{aligned} p_x &= \frac{i}{S} \iint_{\mathrm{BZ}} \langle u(k_x, k_y) | \partial_{k_x} | u(k_x, k_y) \rangle dk_x k_y, \\ p_y &= \frac{i}{S} \iint_{\mathrm{BZ}} \langle u(k_x, k_y) | \partial_{k_y} | u(k_x, k_y) \rangle dk_x k_y, \end{aligned} \tag{7}$$

Optics EXPRESS

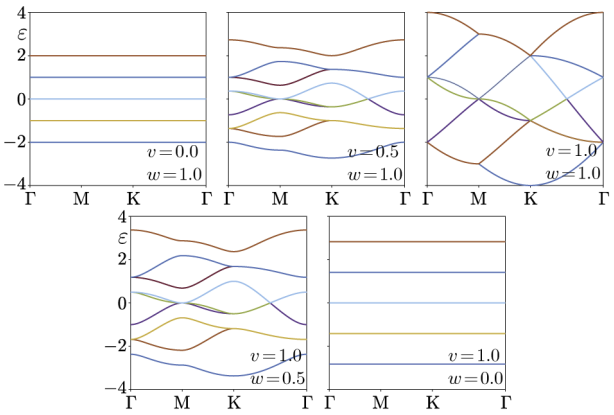

Fig. 4. Dispersion relation of the two-dimensional super-SSH model along high symmetric points, for five settings of hopping amplitude that are given at the right-bottom corner of each panel.

where $S = 4\pi^2$ is the area of the first BZ. Numerical integration on Eq. (7) reveals that the values of p_x and p_y of the top and the bottom bands (i.e., ε_1 and ε_9) are always $1/2$ for $v<w$ and 0 for $v>w$. The result is quite similar to those of the traditional two-dimensional SSH model [45,47,48]. Therefore, one expects to have topological corner states under the condition $v<w$. However, for the case $v>w$, there may be topological defect states too that localize at the corners.

3. Optical realization of the super-SSH model

3.1. One-dimensional case

We provide a possible realization of the super-SSH model in optics/photonics, where the lattice sites can be prepared by using the refractive index change. A light beam $\psi(x, y, z)$ propagating in a certain photonic lattice, $\mathcal{R}(x, y)$, is described by the well-known Schrödinger-like paraxial wave equation:

$$i\frac{\partial\psi}{\partial z} = -\frac{1}{2}\left(\frac{\partial^2}{\partial x^2} + \frac{\partial^2}{\partial y^2}\right)\psi - \mathcal{R}(x, y)\psi, \tag{8}$$

where the transverse (x, y) and longitudinal z-coordinates are normalized to the characteristic transverse scale r_0 and the diffraction length $L_{\text{dif}} = kr_0^2$, respectively; $k = 2\pi n_0/\lambda$ is the wavenumber with n_0 being the background refractive index and λ the wavelength. The lattice potential $\mathcal{R}(x, y) = p\sum_n Q(x-x_n, y)$ is composed of super-Gaussian waveguides $Q = e^{-(x^2+y^2)^2/\sigma^4}$ with p being the depths of two sublattices, σ waveguide widths, and $(x_n, 0)$ the transverse location of each waveguide channel. Such photonic lattices can be created in silicon by using the femto-second laser writing technique [37,49], and typical values for the parameters are $n_0 = 1.45$, $\lambda = 600$ nm, $r_0 = 10$ μm, and $p = 10$ (corresponding to a refractive index change $\sim 6.3 \times 10^{-4}$).

Thus, the three super-SSH chains as shown in Figs. 1(b)–1(d) can be optically mimicked by the waveguide arrays as shown in Figs. 5(a)–5(c). The required variation of coupling coefficient is achieved by controlling the spatial separation between the waveguides. To be specific, we fix a, the length of the unit cell that contains three waveguides within it, and characterize the distance between two adjacent wavgudies to be r. Obviously, for $r = 0.5a$ one has $v = w$, while for $r = 0.6a$ and $r = 0.4a$ one has $v>w$ and $v<w$, respectively. As predicted above, for $r = 0.4a$, there should exist topological edge states, and this is indeed confirmed by rigorously solving the resultant eigen-equation by substituting $\psi(x, y, z) = u(x, y)e^{i\varepsilon z}$ into Eq. (8), and the obtained eigenvalue spectrum is shown in Fig. 5(d) in the region $0.4 \le r/a \le 0.6$. Clearly,

Optics EXPRESS

for r<0.5a, topological edge states appear within two band gaps, as indicated by the red and magenta curves in Fig. 5(d), and exemplified in Fig. 5(a). Such edge modes cover mostly the two outermost waveguides, with modes from the red branch being in-phase between the two occupied waveguides while the modes from the magenta branch being out-of-phase. Note that this property is absent for standard SSH model.

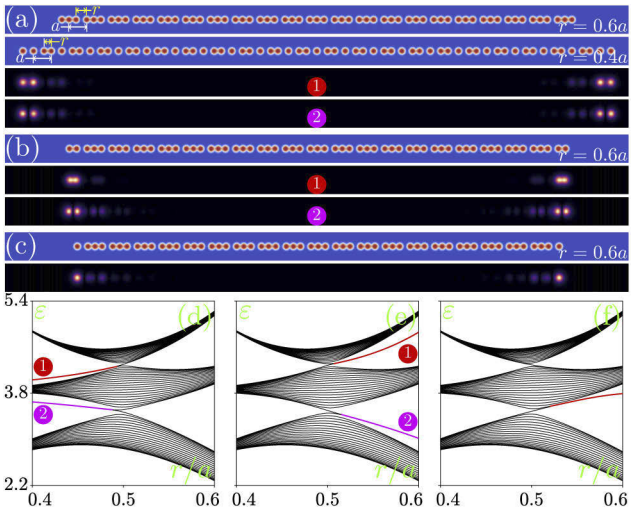

Fig. 5. (a) Two finite photonic super-SSH lattices with complete unit cell with $r = 0.6a$ and $r = 0.4a$. Topological edge states supported in the lattice with $r = 0.4a$, which are corresponding to the red and magenta curves in the band structure shown in (d). (b) One finite photonic super-SSH lattice with $r = 0.6a$ and one site of two boundary unit cells eliminated. Supported topological defect states, which are corresponding to the red and magenta curves in the band structure shown in (e). (c) One finite photonic super-SSH lattice with $r = 0.6a$ and two sites of two boundary unit cells eliminated. Supported topological defect state, which is corresponding to the red curve in the band structure shown in (f). Parameters: $p = 10$, $a = 2.5$ and $\sigma = 0.5$.

It is worth mentioning that the unit cell in the photonic super-SSH lattices in Fig. 5(a) is complete. Ergo, it is interesting to ask what will happen if it is incomplete, namely, some sites at the boundary unit cell are removed? We display such incomplete photonic super-SSH lattices in Figs. 5(b) and 5(c), which corresponds respectively, to the finite super-SSH chains of different boundaries shown in Figs. 1(c) and 1(d). Apparently, one cannot use the winding number predicted by Eq. (5) to characterize the topological phase for these cases any longer. Thus, similar to Fig. 5(d), we calculate directly the eigenvalue spectrum corresponding to the two incomplete super-SSH lattices, and the results are given in Figs. 5(e) and 5(f), respectively. Now, in sharp contrast to the complete unit cell case, for incomplete case, even with r>0.5a, topological edge states are fount to exist in the boundaries [see the red and magenta curves in Figs. 5(e) and 5(f)]. It should be mentioned, however, the localized modes appearing in the region of the incomplete unit cell are topological defect modes (rather than topological boundary modes), and similar situation occurs too in a standard SSH lattice. It should be also mentioned that for the incomplete array Fig. 5(b), topological defect modes appear in both bandgaps [exemplified in lower panels of Fig. 5(b)], while for the incomplete array Fig. 5(c), only the lower bandgap accommodates localized modes.

Optics EXPRESS

3.2. Two-dimensional case

We turn to the two-dimensional case with boundaries as shown in Fig. 6, where the lattice potential is given by $\mathcal{R}(x, y) = p \sum_{n,m} Q(x - x_n, y - y_m)$. As analyzed previously, if $v<w$ there will be topological corner state since the polarization indices are nonzero. Therefore, there should exist topological corner states for the lattice in Fig. 6 if $r<0.5a$. The lattice with $r = 0.4a$ is displayed in Fig. 6(a), while the lattice with $r = 0.6a$ shown in Fig. 6(c). The two lattices corresponding to the cases with $v<w$ and $v>w$, respectively, and the corresponding eigenvalue spectra of the two lattices are shown in Figs. 6(b) and 6(d), respectively. In accordance with previous analysis, there are corner states in Fig. 6(b) (indicated by red circles), but none in Fig. 6(d). Further, In Fig. 6(b), there are three types of corner states (labelled with numbers 1,2, and 3). The modes of the type 1 and 3 reside within the band gaps and are four-folded degenerated, while modes of the type 2 is immersed in the bulk band and are eight-folded degenerated. Typical mode profiles for such three types are presented in Fig. 6(a), just at the right side of the lattice landscape: one from the type 1, one from the type 3, and two from the type 2, as the second type has two difference profiles. One finds that the energy of the corner state from both type 1 and 3 distributes equally on the four corner sites, with the four main humps of the type 1 are in-phase and those of the type 3 are out-of-phase. As to the two different corner states of type 2, they are orthogonal each other, and dipole-like, thus, one can construct vortex-like modes from them [50].

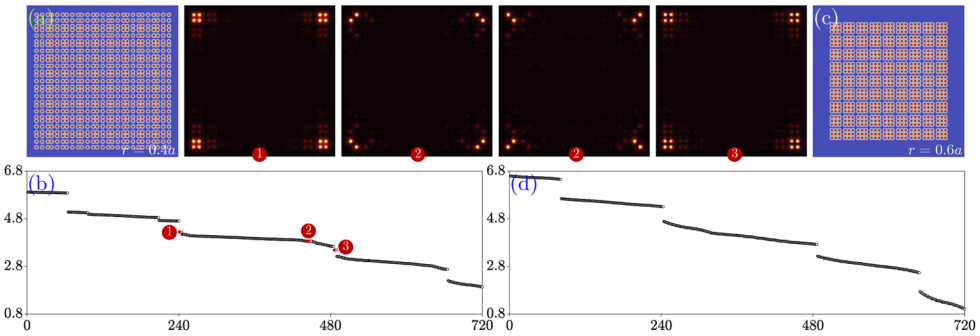

Fig. 6. Two-dimensional super-SSH model (a,c) with different r and corresponding spectra (b,d). Corner states in the spectrum (b) are classified into three types and indicated by red circles. The first and third types have four degenerated corner states, and the second type has eight degenerated corner states that include two orthogonal cases. The corner states from different types are shown in (a).

The lattice in Fig. 6 is complete in the sense that there is no defect and each unit cell has nine sites, and of course one could also have its incomplete versions by removing a few outermost waveguides from the boundaries, expecting the occurrence of the topological defect modes. Taking into account the one-dimensional case where topological defect modes only appear when $r>0.5a$, here for incomplete two-dimensional lattices we also only consider the $r>0.5a$ case. Such lattice landscapes, the respective eigenvalue spectra and the associated corners states are illustrated in Fig. 7. Let us first consider the incomplete lattices by removing the sites along the outermost boundary from the complete structure of Fig. 6(c), which leading to the formation of lattice shown in Fig. 7(a). The corresponding spectrum is shown in Fig. 7(b). One finds that there are indeed topological corner states, which can be also classified into three types, as indicated by red circles. These topological states are quite similar to those shown in Fig. 6. If we further remove the sites along the outer boundary from the lattice shown in Fig. 7(a), the resultant super-SSH model is shown in Fig. 7(c), and the corresponding spectrum is given in Fig. 7(d). In Fig. 7(d), topological corner states are indicated by red circles, but they are in the bulk band. Different from the corner states in the bulk shown in Figs. 6(b) and 7(b), the corner states are not

Optics EXPRESS

four-fold degeneration – the first two are degenerated and the last two are degenerated; the four corner states are exhibited in Fig. 7(c).

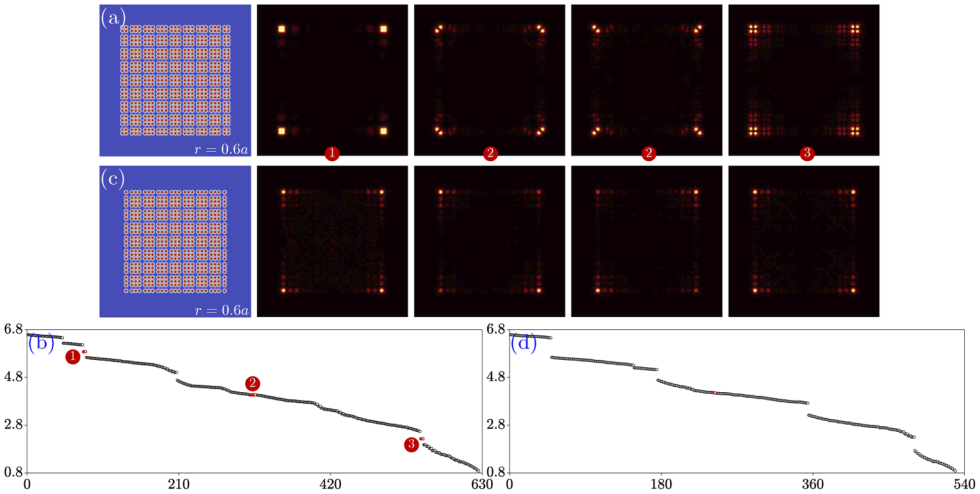

Fig. 7. (a) Two-dimensional super-SSH model with the outer boundary sites of the lattice in Fig. 6(c) eliminated. (b) Spectrum of the lattice in (a) with corner states classified into three types and indicated by red circles. (c) Two-dimensional super-SSH model with the outer boundary sites of the lattice in (a) eliminated. (d) Spectrum of the lattice in (c) with corner states indicated by red circles. Besides the lattice landscape, corner states are also displayed in (a,c). For all the cases, $r = 0.6a$.

4. Conclusion

Summarizing, we have developed the super-SSH model and discussed its topological properties theoretically and numerically. By adjusting the intracell and intercell hopping amplitudes through changing the separation between neighbored sites, we find that either the topological edge state or the topological defect state can be generated in the super-SSH model, and the appearance of the latter one depends how the lattice at the boundary is truncated. The topological edge state appears if the intracell hopping is weaker, however the topological defect states appears if the intracell hopping is stronger. We also extend the super-SSH model into two-dimension, and the nonzero polarization indices indicate that topological corner states will appear in the two-dimensional super-SSH model. Based on the degenerated topological corner dipole-like states, one can produce corner vortex states. We believe that our work may provide a promising platform for fabricating higher-order topological insulators and optical functional devices such as corner lasers [36,43,45]. In addition, the super-SSH model may also serve as a novel candidate for nonlinear topological photonics investigations in different systems [28,31–33,37,51–53].

Funding. National Natural Science Foundation of China (12074308, U1537210); Fundamental Research Funds for the Central Universities (xzy012019038).

Disclosures. The authors declare no conflicts of interest.

Data availability. Data underlying the results presented in this paper are not publicly available at this time but may be obtained from the authors upon reasonable request.

References

1. M. Z. Hasan and C. L. Kane, "Colloquium: Topological insulators," Rev. Mod. Phys. **82**(4), 3045–3067 (2010).
2. X.-L. Qi and S.-C. Zhang, "Topological insulators and superconductors," Rev. Mod. Phys. **83**(4), 1057–1110 (2011).
3. J. K. Asbóth, L. Oroszlány, and A. Pályi, *The Su-Schrieffer-Heeger (SSH) Model* (Springer, Cham, 2016), pp. 1–22.

Optics EXPRESS

4. A. Blanco-Redondo, I. Andonegui, M. J. Collins, G. Harari, Y. Lumer, M. C. Rechtsman, B. J. Eggleton, and M. Segev, "Topological optical waveguiding in silicon and the transition between topological and trivial defect states," Phys. Rev. Lett. **116**(16), 163901 (2016).
5. H. Deng, X. Chen, N. C. Panoiu, and F. Ye, "Topological surface plasmons in superlattices with changing sign of the average permittivity," Opt. Lett. **41**(18), 4281–4284 (2016).
6. W.-F. Zhang, C.-Y. Li, X.-F. Chen, C.-M. Huang, and F.-W. Ye, "Topological zero-energy modes in time-reversal-symmetry-broken systems (in Chinese)," Acta Phys. Sin. **66**(22), 220201 (2017).
7. P. St-Jean, V. Goblot, E. Galopin, A. Lemaître, T. Ozawa, L. Le Gratiet, I. Sagnes, J. Bloch, and A. Amo, "Lasing in topological edge states of a one-dimensional lattice," Nat. Photonics **11**(10), 651–656 (2017).
8. M. Parto, S. Wittek, H. Hodaei, G. Harari, M. A. Bandres, J. Ren, M. C. Rechtsman, M. Segev, D. N. Christodoulides, and M. Khajavikhan, "Edge-mode lasing in 1D topological active arrays," Phys. Rev. Lett. **120**(11), 113901 (2018).
9. H. Zhao, P. Miao, M. H. Teimourpour, S. Malzard, R. El-Ganainy, H. Schomerus, and L. Feng, "Topological hybrid silicon microlasers," Nat. Commun. **9**(1), 981 (2018).
10. S. Longhi, "Probing one-dimensional topological phases in waveguide lattices with broken chiral symmetry," Opt. Lett. **43**(19), 4639–4642 (2018).
11. Q. Cheng, Y. Pan, H. Wang, C. Zhang, D. Yu, A. Gover, H. Zhang, T. Li, L. Zhou, and S. Zhu, "Observation of anomalous π modes in photonic Floquet engineering," Phys. Rev. Lett. **122**(17), 173901 (2019).
12. D. Leykam and D. A. Smirnova, "Probing bulk topological invariants using leaky photonic lattices," Nat. Phys. **17**(5), 632–638 (2021).
13. Y. Ota, K. Takata, T. Ozawa, A. Amo, Z. Jia, B. Kante, M. Notomi, Y. Arakawa, and S. Iwamoto, "Active topological photonics," Nanophotonics **9**(3), 547–567 (2020).
14. S. Longhi, "Topological Anderson phase in quasi-periodic waveguide lattices," Opt. Lett. **45**(14), 4036–4039 (2020).
15. D. T. H. Tan, "Topological silicon photonics," Adv. Photonics Res. **2**(9), 2100010 (2021).
16. M. Esmann, F. R. Lamberti, A. Lemaître, and N. D. Lanzillotti-Kimura, "Topological acoustics in coupled nanocavity arrays," Phys. Rev. B **98**(16), 161109 (2018).
17. X. Li, Y. Meng, X. Wu, S. Yan, Y. Huang, S. Wang, and W. Wen, "Su-Schrieffer-Heeger model inspired acoustic interface states and edge states," Appl. Phys. Lett. **113**(20), 203501 (2018).
18. M. Atala, M. Aidelsburger, J. T. Barreiro, D. Abanin, T. Kitagawa, E. Demler, and I. Bloch, "Direct measurement of the Zak phase in topological Bloch bands," Nat. Phys. **9**(12), 795–800 (2013).
19. B. X. Wang and C. Y. Zhao, "Topological photonic states in one-dimensional dimerized ultracold atomic chains," Phys. Rev. A **98**(2), 023808 (2018).
20. D.-W. Zhang, Y.-Q. Zhu, Y. X. Zhao, H. Yan, and S.-L. Zhu, "Topological quantum matter with cold atoms," Adv. Phys. **67**(4), 253–402 (2018).
21. Y. Wang, Y.-H. Lu, F. Mei, J. Gao, Z.-M. Li, H. Tang, S.-L. Zhu, S. Jia, and X.-M. Jin, "Direct observation of topology from single-photon dynamics," Phys. Rev. Lett. **122**(19), 193903 (2019).
22. F. M. D'Angelis, F. A. Pinheiro, D. Guéry-Odelin, S. Longhi, and F. Impens, "Fast and robust quantum state transfer in a topological Su-Schrieffer-Heeger chain with next-to-nearest-neighbor interactions," Phys. Rev. Res. **2**(3), 033475 (2020).
23. E. J. Meier, F. A. An, and B. Gadway, "Observation of the topological soliton state in the Su-Schrieffer-Heeger model," Nat. Commun. **7**(1), 13986 (2016).
24. M. Pan, H. Zhao, P. Miao, S. Longhi, and L. Feng, "Photonic zero mode in a non-Hermitian photonic lattice," Nat. Commun. **9**(1), 1308 (2018).
25. Z. Turker, S. Tombuloglu, and C. Yuce, "PT symmetric Floquet topological phase in SSH model," Phys. Lett. A **382**(30), 2013–2016 (2018).
26. S. Longhi, "Non-Hermitian gauged topological laser arrays," Ann. Phys. **530**(7), 1800023 (2018).
27. S. R. Pocock, P. A. Huidobro, and V. Giannini, "Bulk-edge correspondence and long-range hopping in the topological plasmonic chain," Nanophotonics **8**(8), 1337–1347 (2019).
28. S. Xia, D. Kaltsas, D. Song, I. Komis, J. Xu, A. Szameit, H. Buljan, K. G. Makris, and Z. Chen, "Nonlinear tuning of PT symmetry and non-Hermitian topological states," Science **372**(6537), 72–76 (2021).
29. S. Lieu, "Topological phases in the non-Hermitian Su-Schrieffer-Heeger model," Phys. Rev. B **97**(4), 045106 (2018).
30. X. Zhou, Y. Wang, D. Leykam, and Y. D. Chong, "Optical isolation with nonlinear topological photonics," New J. Phys. **19**(9), 095002 (2017).
31. M. Guo, S. Xia, N. Wang, D. Song, Z. Chen, and J. Yang, "Weakly nonlinear topological gap solitons in Su-Schrieffer-Heeger photonic lattices," Opt. Lett. **45**(23), 6466–6469 (2020).
32. A. Y. Zykin, D. V. Skryabin, and Y. V. Kartashov, "Topological solitons in arrays of modelocked lasers," Opt. Lett. **46**(9), 2123–2126 (2021).
33. S. Xia, D. Jukić, N. Wang, D. Smirnova, L. Smirnov, L. Tang, D. Song, A. Szameit, D. Leykam, J. Xu, Z. Chen, and H. Buljan, "Nontrivial coupling of light into a defect: the interplay of nonlinearity and topology," Light: Sci. Appl. **9**(1), 147 (2020).
34. B. Xie, H.-X. Wang, X. Zhang, P. Zhan, J.-H. Jiang, M. Lu, and Y. Chen, "Higher-order band topology," Nat. Rev. Phys. **3**(7), 520–532 (2021).
35. Y. Zhang, Y. V. Kartashov, L. Torner, Y. Li, and A. Ferrando, "Nonlinear higher-order polariton topological insulator," Opt. Lett. **45**(17), 4710–4713 (2020).

Optics EXPRESS

36. H. Zhong, Y. V. Kartashov, A. Szameit, Y. Li, C. Liu, and Y. Zhang, "Theory of topological corner state laser in Kagome waveguide arrays," APL Photonics **6**(4), 040802 (2021).
37. M. S. Kirsch, Y. Zhang, M. Kremer, L. J. Maczewsky, S. K. Ivanov, Y. V. Kartashov, L. Torner, D. Bauer, A. Szameit, and M. Heinrich, "Nonlinear second-order photonic topological insulators," Nat. Phys. **17**(9), 995–1000 (2021).
38. C. Li, F. Ye, X. Chen, Y. V. Kartashov, A. Ferrando, L. Torner, and D. V. Skryabin, "Lieb polariton topological insulators," Phys. Rev. B **97**(8), 081103 (2018).
39. D. Leykam, A. Andreanov, and S. Flach, "Artificial flat band systems: from lattice models to experiments," Adv. Phys.: X **3**(1), 1473052 (2018).
40. K. C. Jin, H. Zhong, Y. D. Li, F. W. Ye, Y. P. Zhang, F. L. Li, C. L. Liu, and Y. Q. Zhang, "Parametric type-II Dirac photonic lattices," Adv. Quantum Technol. **3**(7), 2000015 (2020).
41. V. M. Martinez Alvarez and M. D. Coutinho-Filho, "Edge states in trimer lattices," Phys. Rev. A **99**(1), 013833 (2019).
42. Y. He and C.-C. Chien, "Non-Hermitian generalizations of extended Su-Schrieffer-Heeger models," J. Phys.: Condens. Matter **33**(8), 085501 (2021).
43. W. Zhang, X. Xie, H. Hao, J. Dang, S. Xiao, S. Shi, H. Ni, Z. Niu, C. Wang, K. Jin, X. Zhang, and X. Xu, "Low-threshold topological nanolasers based on the second-order corner state," Light: Sci. Appl. **9**(1), 109 (2020).
44. C. Han, M. Kang, and H. Jeon, "Lasing at multidimensional topological states in a two-dimensional photonic crystal structure," ACS Photonics **7**(8), 2027–2036 (2020).
45. H.-R. Kim, M.-S. Hwang, D. Smirnova, K.-Y. Jeong, Y. Kivshar, and H.-G. Park, "Multipolar lasing modes from topological corner states," Nat. Commun. **11**(1), 5758 (2020).
46. D. Xiao, M.-C. Chang, and Q. Niu, "Berry phase effects on electronic properties," Rev. Mod. Phys. **82**(3), 1959–2007 (2010).
47. B.-Y. Xie, H.-F. Wang, H.-X. Wang, X.-Y. Zhu, J.-H. Jiang, M.-H. Lu, and Y.-F. Chen, "Second-order photonic topological insulator with corner states," Phys. Rev. B **98**(20), 205147 (2018).
48. B.-Y. Xie, G.-X. Su, H.-F. Wang, H. Su, X.-P. Shen, P. Zhan, M.-H. Lu, Z.-L. Wang, and Y.-F. Chen, "Visualization of higher-order topological insulating phases in two-dimensional dielectric photonic crystals," Phys. Rev. Lett. **122**(23), 233903 (2019).
49. D. Tan, Z. Wang, B. Xu, and J. Qiu, "Photonic circuits written by femtosecond laser in glass: improved fabrication and recent progress in photonic devices," Adv. Photonics **3**(2), 024002 (2021).
50. K. C. Jin, Y. D. Li, F. Li, M. R. Belić, Y. P. Zhang, and Y. Q. Zhang, "Rabi oscillations of azimuthons in weakly nonlinear waveguides," Adv. Photonics **2**(4), 046002 (2020).
51. Y. V. Kartashov, G. E. Astrakharchik, B. A. Malomed, and L. Torner, "Frontiers in multidimensional self-trapping of nonlinear fields and matter," Nat. Rev. Phys. **1**(3), 185–197 (2019).
52. B. A. Malomed and D. Mihalache, "Nonlinear waves in optical and matter-wave media: A topical survey of recent theoretical and experimental results," Rom. J. Phys. **64**, 106 (2019).
53. D. Mihalache, "Localized structures in optical and matter-wave media: A selection of recent studies," Rom. Rep. Phys. **73**, 403 (2021).